New Method for Supersonic Boundary-Layer Separations

M. J. WERLE* AND V. N. VATSA†
University of Cincinnati, Cincinnati, Ohio

An efficient numerical solution algorithm is presented for solving the interacting supersonic laminar boundary-layer problem. The method employs a time dependent approach with the alternating direction implicit (ADI) scheme and directly accounts for the necessary downstream boundary condition. Solutions are presented for $M_\infty = 3$ cold wall boundary-layer flow over a family of compression ramps with regions of reverse flow. Good comparison is given with experimental data and Navier-Stokes solutions for $M_\infty = 4$ and 6, adiabatic wall, separated flow up a 10° compression ramp.

Nomenclature

B = constant for ramp geometry, see Fig. 1
C = constant for ramp geometry, see Fig. 1
C_f = skin friction coefficient, wall shear $\div \rho_\infty U_\infty{}^2$
$\bar{C}_f$ = normalized skin-friction coefficient, $\bar{C}_f = C_f(Re)^{1/2}$
$\bar{e}$ = constant in coefficient of artificial time terms, here $\bar{e} = \frac{1}{30}$
F = normalized longitudinal velocity, $F = u/U$
h = coefficient of artificial time terms, see Eqs. (10) and (11)
h^* = coefficient of artificial time terms, see Eqs. (10) and (11)
k_p = grouping of inviscid terms in pressure gradient parameter, β
l = viscosity function, $l = \rho\mu/\rho_e\mu_e$
L = reference length
M = Mach number
n = coordinate normal to surface
N = stretched normal coordinate, $N = n/\varepsilon$
p = pressure
$\bar{Q}$ = wall heat-transfer coefficient, heat transfer $\cdot (Re)^{1/2}/\rho_\infty U_\infty{}^3$
r_o = transverse radius of curvature for axisymmetric body
R = universal gas constant
Re = reference Reynolds number, $Re = \rho_\infty U_\infty L/\mu(T_r)$
Re_∞ = freestream Reynolds number
s = longitudinal surface distance
t = time
T = temperature
T_r = reference temperature, $U_\infty{}^2/R$
u = longitudinal velocity component in boundary layer
U = longitudinal velocity component in inviscid flow
V = normal velocity component in boundary layer
$\bar{X}$ = Cartesian coordinate, see Fig. 1
Y = Cartesian coordinate, see Fig. 1
α = $U_e{}^2/T_e$
β = pressure gradient parameter for boundary-layer equations
$\bar{\beta}$ = $\bar{\beta} = \beta + h\,\partial\delta/\partial t$
γ_1, γ_2 = convenient functional groupings for δ equation
δ = displacement thickness
δ_1 = constant in separation point expansion
Δ = difference increment
ε = $1/(Re)^{1/2}$
μ = viscosity
η = transformed normal coordinate
ρ = density
σ = Prandtl number
θ = normalized temperature, $\theta = T/T_e$
$\bar{\theta}_s$ = local inclination angle of surface
θ_R = asymptotic ramp angle, see Fig. 1
ξ = transformed longitudinal coordinate

Superscripts

j = $j = 0$ for two-dimensional flow, $j = 1$ for axisymmetric flow
n = time level
$*$ = time level $t^n + \Delta t/2$ or dimensional quantity

Subscripts

aw = adiabatic wall
e = inviscid edge value
i = index for longitudinal grid location
j = index for normal grid location
s = separation point
w = wall value
∞ = freestream conditions
INV = inviscid solution only

Introduction

THE problem of boundary-layer separation from a surface in high speed flight continues to be of interest to the fluid dynamicists. Since the separation phenomenon leads to severe surface heating problems and troublesome center-of-pressure shifts, the predictability of such events is critical to improved vehicle design. Considerable success has been experienced in recent years by investigators using numerical methods to solve the interacting boundary-layer equations.[1-10] To date though, nearly all such efforts suffer two deficiencies that limit their general acceptance. The first difficulty centers around their approximate nature. Most such studies either approximate the boundary-layer model itself (as do Refs. 6–9 in the reverse flow regions) or generate approximate solutions to the full boundary-layer model.[1-5]

The second limitation of previous methods comes about due to the boundary value nature of the problem itself. The interacting boundary-layer equations are of the boundary value type and thus require statement of some downstream boundary condition for proper closure of the problem.[11-14] Most methods to date have had to account for the downstream conditions (sometimes referred to as the downstream compatibility condition) in an iterative manner. This is usually accomplished through repeated iteration on one of the parameters of the problem at the upstream boundary to obtain a solution that proceeds smoothly to the downstream boundary. Such "shooting" techniques have proven to be rather costly and time consuming due to the extreme sensitivity of the solutions to minute changes in the upstream state. The recent study of subsonic separations by Kuhn and Nielsen[10] presents a relaxation technique for direct accounting of downstream conditions but the method is still in an embryonic state.

The goal of the present effort was to develop a practical numerical algorithm for solving the two-dimensional laminar interacting supersonic boundary-layer equations (when regions of reverse flow are present) with direct accounting made of the downstream compatibility conditions. To this end a relaxation

Received November 7, 1973; revision received June 3, 1974. This work was supported by the U.S. Air Force through the Hypersonic Research Laboratory under Contract F 33615-73-C-4014.

Index categories: Boundary Layers and Convective Heat Transfer—Laminar; Jets, Wakes, and Viscid-Inviscid Flow Interactions.

* Associate Professor, Department of Aerospace Engineering. Associate Member AIAA.

† Graduate Research Assistant, Department of Aerospace Engineering.

scheme is presented which employs an alternating direction implicit approach. Detailed solutions are presented for $M = 3$, while at $M = 4$ and 6, surface pressure comparisons are made with experimental data and previously published numerical solutions for the full Navier-Stokes equations. For all cases presented here the computer time needed on an IBM 370-165 computer using finite difference grids with up to 16000 mesh points was on the order of 15 min for attainment of results converged within plotting accuracy.‡

Governing Equations

It is assumed that the boundary-layer equations are adequate for the interaction problems of interest here. Such an assumption only seems questionable in the case of separated flow where one might suspect that more terms of the Navier-Stokes equations might have to be retained. However, Stewartson and Williams[15] have recently addressed this question and shown through a new asymptotic analysis for large Reynolds number that a boundary-layer like set of equations still governs the flow process that accompanies the free interaction pressure rise through a supersonic separation point. Similar studies have been presented by Melnik et al.,[16] and Brillant et al.[17] for the transonic flow problem. One interesting point about this new equation set is that it contains no new viscous terms over those included in Prandtl's equations. Thus, the boundary-layer model can be retained for both attached and separated flows and these are employed here in terms of the Levy-Lees variables

$$\xi = \int_o^s \rho_e \mu_e U_e r_o^{2j}\, ds \qquad \eta = \frac{U_e r_o^j}{(2\xi)^{1/2}} \int_o^N \rho\, dN \tag{1}$$

where all variables have been nondimensionalized with the freestream density, $\rho_\infty{}^*$, the freestream velocity, $U_\infty{}^*$, a reference length, L^*, and a reference temperature, $T_r{}^* = U_\infty{}^{*2}/R$ with R being the gas constant. In addition, the physical coordinate normal to the surface, n, has been stretched according to the usual scheme $n = N/(Re)^{1/2} = \varepsilon N$.

Normalizing the longitudinal velocity and static temperature as

$$F = u/U_e \tag{2}$$

and

$$\theta = T/T_e \tag{3}$$

and defining a transformed normal velocity equivalent as

$$V = \left[\frac{\partial \eta}{\partial s} F + \rho r_o{}^j v/(2\xi)^{1/2}\right] 2\xi \Big/ \frac{d\xi}{ds} \tag{4}$$

leads to the equation set

$$V_\eta + F + 2\xi F_\xi = 0 \tag{5a}$$

$$(lF_\eta)_\eta - VF_\eta + \beta(\theta - F^2) - 2\xi F F_\xi = 0 \tag{5b}$$

$$\frac{1}{\sigma}(l\theta_\eta)_\eta - V\theta_\eta + \alpha F_\eta{}^2 - 2\xi F \theta_\xi = 0 \tag{5c}$$

where

$$l = \rho\mu/\rho_e\mu_e, \quad \alpha = U_e{}^2/T_e, \quad \beta = \frac{2\xi}{U_e}\frac{dU_e}{d\xi} \tag{5d}$$

The wall boundary conditions are given as

$$F(\xi, 0) = V(\xi, 0) = 0 \quad \theta(\xi, 0) = T_w/T_e \tag{6}$$

Determination of the inviscid edge conditions is not at all obvious. So long as the boundary layer is not separated, arguments based on Van Dyke's higher order boundary-layer theory[18] can be invoked. For this case, Davis, Werle, and Wornom[19] have given the general matching conditions that must be employed. However for ease of application, it is more convenient to employ a "displacement body" concept, in which the influence of the boundary-layer growth on the inviscid stream is modeled as inviscid flow on the surface formed by adding the classically defined displacement thickness to the original surface geometry. While the approach seems more descriptive than analytical in nature, it can be shown to be formally correct for the second-order boundary-layer equations (see Ref. 20 for a discussion of the incompressible case) by simply asking where the inviscid stream-function vanishes. Since higher order boundary-layer concepts must hold fore and aft of a separation bubble, and Stewartson and Williams' model[15] implies the boundary-layer model applies near separation, it does not seem unreasonable to even apply this model throughout the separation region.

For present purposes then, the inviscid flow is taken to be an isentropic flow over the displacement body with the local pressure level obtained from linear theory§ as

$$p_e = p_\infty + \left(\bar{\theta}_s + \varepsilon \frac{d\delta}{ds}\right) \Big/ (M_\infty{}^2 - 1)^{1/2} \tag{7a}$$

where

$$\delta = \int_o^\infty \left(1 - \frac{\rho u}{\rho_e U_e}\right) dN = \frac{(2\xi)^{1/2}}{\rho_e U_e r_o{}^j} \int_o^\infty (\theta - F)\, d\eta \tag{7b}$$

With this approximation, the pressure gradient parameter, β, of Eq. (5d) becomes

$$\beta = -k_p \left[\frac{d\bar{\theta}_s}{ds} + \varepsilon \frac{d^2\delta}{ds^2}\right] \tag{8a}$$

where

$$k_p = \frac{2\xi}{\rho_e{}^2 \mu_e U_e{}^3 r_o{}^{2j}} \Big/ (M_\infty{}^2 - 1)^{1/2} \tag{8b}$$

Inclusion of this last expression coupling the inviscid and viscous flows changes the entire nature of the boundary-layer problem. Whereas the inviscid flow problem is a hyperbolic one, and the viscous flow is a parabolic one, coupling the two flows leads to a boundary value problem (see Garvine,[12] Werle, Dwoyer, and Hankey,[14] or Werle and Vatsa,[30] for further discussion of this point). Thus, to complete the statement of the problem, both initial and final conditions must be identified. For present purposes the leading edge will always be taken as a flat plate, and it is assumed that at some convenient point along the surface, the true solution is only slightly departed from the usual flat plate profile.

Considering the downstream final condition, for the configurations of interest here the boundary layer should asymptotically approach a constant pressure self-similar state. For present purposes this was accomplished by setting the pressure gradient at its inviscid level at some point well aft of the reattachment point. The following section describes a new relaxation technique that allows direct accounting of this necessary boundary condition.

Numerical Analysis—An Alternating Direction Implicit Scheme

To facilitate development of a relaxation process for solving the interacting boundary-layer problem, an artificial time like term is introduced into the momentum equation through the pressure gradient term (see Ref. 21 for a description of the ADI approach). Thus, the term β of Eq. (5b) is replaced by the term $\bar{\beta}$ defined as

$$\bar{\beta} \equiv \beta + h(\partial\delta/\partial t) \tag{9}$$

where h is a variable that will be defined shortly. The numerical solution to the boundary-layer equations now proceeds in increments of time, Δt, with each step divided into two half increments.

During the first step (the * step) Eq. (5b) with Eq. (9) is progressed from time t^n to time $t^* = t^n + \Delta t/2$, using a backward

‡ Recent minor changes in the algorithm has reduced the computer effort needed to 5 min for the same level of accuracy.

§ For higher Mach numbers, this is replaced with the tangent wedge law with no new complications.

difference to represent $\partial\delta/\partial t$, evaluating $\partial^2\delta/\partial s^2$ at time t^n using central differences, and evaluating all other terms at t^* to give

$$(l^*F_\eta^*)_\eta - V^*F_\eta^* + (F^{*2}-\theta^*)\left[k_p^*\frac{d\bar{\theta}_s}{ds} + \varepsilon k_p^*\frac{\partial^2\delta^n}{\partial s^2} - \frac{h^*\delta^*}{\Delta t/2} - \frac{h\delta^n}{\Delta t/2}\right] - 2\xi^*F^*F_\xi^* = 0 \qquad (10)$$

In this form Eq. (10) appears as a spatially parabolic partial differential equation and can be solved very effectively by marching in the ξ-direction using a spatially implicit finite difference scheme. Central differences are used to represent η derivatives and a backward difference for the ξ derivative resulting in an easily inverted tridiagonal set of algebraic equations. The continuity and energy equations do not contain any time like terms and are evaluated simultaneously with the momentum equation, i.e., at $t^* = t^n + \Delta t/2$. These are solved using the now popular implicit approach laid down by Flügge-Lotz and Blottner.[22]

Once a sweep in the ξ-direction has been completed, the second half time step is taken by evaluating, a) $\partial^2\delta/\partial s^2$ at time $t^{n+1} = t^* + \Delta t/2$ using central differences, b) $\partial\delta/\partial t$ as a backward difference over the half time step $\Delta t/2$, and c) all other terms at time t^*. Since this equation holds for all η, it can be evaluated at any convenient location, here taken to be $\eta = 0$. Under these restrictions, the second half time sweep becomes

$$\frac{\partial^2\delta^{n+1}}{\partial s^2} + \gamma_1(\xi)\delta^{n+1} = \gamma_2(\xi) \qquad (11a)$$

where

$$\gamma_1(\xi) = (-2h/\varepsilon k_p^*\Delta t) \qquad (11b)$$

$$\gamma_2(\xi) = (l^*F_\eta^*)_{\eta_w}/(\varepsilon k_p^*\theta_w^*) - \frac{2h^*\delta^*}{\varepsilon k_p^*\Delta t} - \frac{1}{\varepsilon}\frac{d\bar{\theta}_s}{ds} \qquad (11c)$$

This relation is quite easily solved using a central difference approximation which again produces a tridiagonal set of algebraic equations.

It remains now to determine the appropriate form of the time term coefficients, h and h^*. These are chosen here to remove a fundamental singularity encountered whenever regions of separated flow occur. Once there are regions of separated flow, the familiar square-root type of singularity is encountered near separation.[23] The reason the singular behavior enters the problem even though interaction effects are included is found in the alternating direction algorithm itself. Note from Eq. (10), that the contribution of the interaction process to the pressure gradient enters through the term, δ_{ss}, and that this is evaluated at time t^n during the * time sweep. In a sense then, the boundary-layer is developing under a prescribed pressure gradient and, as verified by Werle and Senechal,[24] one must always expect to encounter a square-root singularity at the zero skin friction point for this situation. Based on the work of many previous investigators (see Buckmaster,[25] for detailed discussion) and the numerical studies of Werle and Senechal,[24] it is now apparent that near separation, the principal behavior of the displacement thickness is characterized as

$$\delta \sim \delta_s + (s_s - s)^{1/2}\delta_1 \qquad (12a)$$

with

$$\delta' \sim \tfrac{1}{2}(s_s - s)^{-1/2}\delta_1 \qquad (12b)$$

and

$$\frac{d^2\delta}{d\delta^2} = \delta'' \sim \tfrac{1}{4}(s_s - s)^{-3/2}\delta_1 \sim \delta'^3 \qquad (12c)$$

This last expression is of interest for it shows that δ'' is highly singular at separation if the pressure gradient is fully prescribed. However, it is well documented[1-10] that the governing equations will not let this singularity emerge if the δ'' is allowed to self adjust through interaction with the mainstream. Thus, to remove the singularity in the present formulation, one need only introduce a term that would have a singularity of the form shown in Eq. (12c) if interaction was not accounted for and to let this term be evaluated during the * time step through the interaction model. Such a term is not at all unique in character and many different candidates have been considered. It was found that taking h and h^* proportional to δ'^3 [which from Eq. (12c) has the sought-after character] removed the singularity entirely and allowed easy passage into the reverse flow region. The form of the multipliers found to remove the singularity and maintain stability were

$$h = \left[\frac{1-\bar{e}\delta'^*}{1-\bar{e}\delta'^n}\right]^3 \qquad (13a)$$

and

$$h^* = \left[\frac{1+\bar{e}\delta'^*}{1+\bar{e}\delta'^n}\right]^3 \qquad (13b)$$

where the constant $\bar{e}$ was here taken to be $\frac{1}{30}$. Note that in this form these multipliers are close to unity for all finite time levels and exactly approach unity as $t \to \infty$. In addition, for the case of a prescribed pressure gradient both h and h^* would have the proper form of the singularity and thus serve to keep such from emerging during the star sweep.

Two further adjustments to the algorithm were necessary in order to proceed with separated flow studies. In regions of reverse flow, the algorithm encounters an instability due to the reversal of the longitudinal velocity convective term. To overcome this an upwind difference scheme was employed. In this approach, whenever the velocity component F was less than zero, a staggered forward difference was used to represent the convective term $\partial F/\partial\xi$. Thus, during the star time step the finite difference representation of the convective term is given as

$$F^*F_\xi^* = \frac{F^*+|F^*|}{2}\left(\frac{F_i^* - F_{i-1}^*}{\Delta\xi}\right) + \frac{F^*-|F^*|}{2}\left(\frac{F_{i+1}^n - F_i^*}{\Delta\xi}\right) \qquad (14)$$

A von Neumann stability analysis shows this to be unconditionally stable.

The second adjustment employed a change in the algorithm necessary in order to obtain reverse flow profiles to the boundary-layer equations. Following the approach introduced by Werle and Bertke[26] and applied by Werle et al.[7,8] the continuity equation coupled directly to the momentum equation through quasilinearization has been integrated from its outer edge into the wall with iteration on V_e to achieve $V_w = 0$. This approach provides a stable base for calculating profiles with regions of reverse flow.

Numerical solution of the star step equations follows closely the approach outlined by Blottner[27] and that employed by Werle et al.[7] The procedure iterates at each longitudinal station in order to assure that the interaction process is properly accounted for.

The iterative solution procedure starts by solving the energy equation by linearizing the convective and viscosity terms using the previous station velocity and temperature profiles. The viscosity coefficient is updated and the momentum equation coupled with continuity is then solved. The value of δ^* is calculated using these profiles and then $\partial\delta^*/\partial s$ is obtained using a backward difference law. Inviscid edge quantities are evaluated using this value of $\partial\delta^*/\partial s$ and the process is repeated until δ^* converges to some prescribed tolerance. The new guesses on δ^* were generated from a Newton-Raphson iteration scheme. In regions of large longitudinal gradients it was not always possible to converge the nonlinear coefficients of Eq. (10) simultaneously with the δ^* iteration. At such stations the nonlinear terms were first relaxed completely before making a new guess on δ^*. In addition, in regions of reverse flow an additional iterative loop is added to obtain a value of V_e that produces a value of $V = 0$ at the wall.

Note that the present formulation requires a guess on the zero time level displacement thickness, δ^n, all along the s-direction. It was observed during calculations that any smooth distribution, e.g., a square root or a linear variation of displacement thickness could be used as a first guess without causing a significant effect on the final solution.

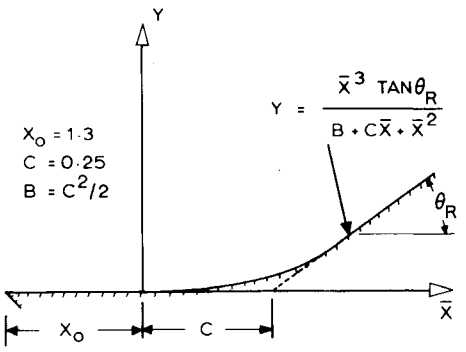

Fig. 1 Ramp geometry.

Results and Discussion

All of the test cases involved flow over a compression ramp with sufficiently high angles to induce separation. The initial test conditions considered were $M_\infty = 3.0$, $Re_\infty = 10^5$, $T_w/T_{o_\infty} = 0.5$, $T_\infty = 100°F$ for flow up the ramp geometry given in Fig. 1. In this study the ramp corner was placed at $s = 1.55$ with $x_o = 1.3$ and $c = 0.25$. Solutions are presented for ramp angles from 9° to 12° in 1° increments.

For the compression ramps discussed here, use is made of self-similar solutions with a small pressure rise (say, 1%) as the upstream boundary condition, whereas $\delta'' = 0$ is used as the downstream boundary conditions (which is equivalent to setting the induced pressure gradient equal to zero at the downstream end).

The distributions of inviscid surface pressure, resulting surface pressure, skin friction, and heat transfer rates for this set of ramps are presented in Figs. 2–5. These calculations were performed with the longitudinal step size $\Delta s = 0.01$ and each case consumed approximately 15–30 min of computer time on an IBM 370-165 machine to perform between 10 and 15 time iterations. Attention is called to the fact that these solutions were initiated at $s = 0.8$ to insure that a respectable region of weak interaction was first traversed in order to purge any errors introduced by the initial station assumptions.

Of immediate interest are the skin friction distributions shown in Fig. 4, where a smooth departure from the weak interaction solution leads quickly to a nonsingular pass through separation and reattachment. The rapid growth of the separation bubble as the ramp angle is increased is not surprising for a laminar boundary layer. However, this behavior does force one to consider very large mesh regions in order to be able to place the requirement of a zero induced pressure gradient at some downstream station. From Fig. 4 it is obvious that the 12° ramp angle case may not yet be correctly modeled since the skin friction had not yet started on its downstream weak interaction

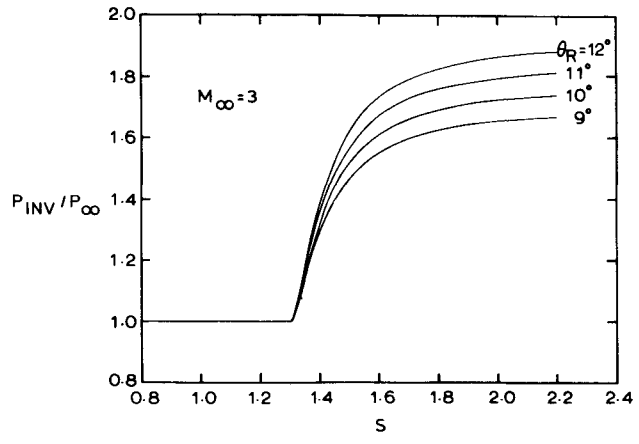

Fig. 2 Inviscid pressure distributions for compression ramps.

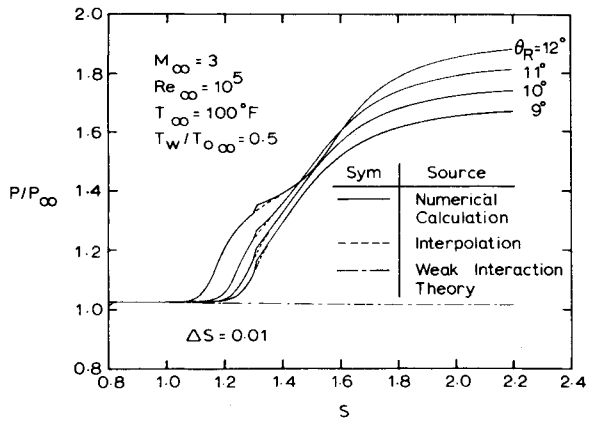

Fig. 3 Interaction pressure distributions for compression ramps.

decay by the $s = 2.2$ station (which it of course should as $s \to \infty$). Even though the error in placing the downstream boundary condition too close to the strong interaction region did not produce any pathological behavior here, this was not always the case. It was observed in several other studies that, when the downstream boundary condition was placed too far forward, the algorithm could not overcome the error so induced and would not converge to a steady state solution. Thus, quite naturally, care must be exercised in establishing the level and position of the downstream boundary condition.

The pressure distributions accompanying the skin friction curves of Fig. 4 are presented in Fig. 3. Note that all of these curves show a "Kink" in the pressure levels at the station immediately aft of the point where the ramp begins ($s = 1.3$). These "Kinks" are due to truncation errors in the finite difference approximation to the second derivative of the displacement thickness appearing in Eq. (8a). They are easily removed by either reducing the longitudinal step size or by representing the pressure gradient term by a finite difference approximation to the second derivative of the displacement body height formed by adding δ to the ramp surface height Y.

The heat transfer distributions of Fig. 5 follow the expected behavior, showing a drastic drop over the same region for which the skin friction drops. Attention is directed to the "wiggles" in the local heating rates aft of the separation points. These are due to errors in the numerical algorithm induced by the fact the value of the velocity normal to the wall is only zero to within a finite tolerance (recall the zero injection condition is satisfied here iteratively) which can be tightened to remove this behavior if need be.

For the ramp angle range considered in Figs. 2–5, solutions have also been obtained with a longitudinal step size increased from 0.01 to 0.02. A first point of concern is whether or not solutions different from the weak interaction solution could be generated. Previous studies[14] found that "shooting techniques"

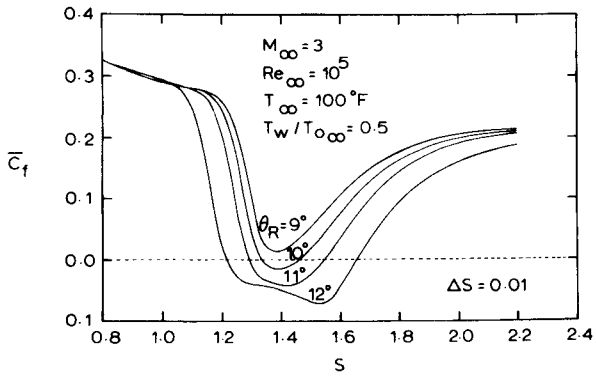

Fig. 4 Interaction skin-friction distributions for compression ramps.

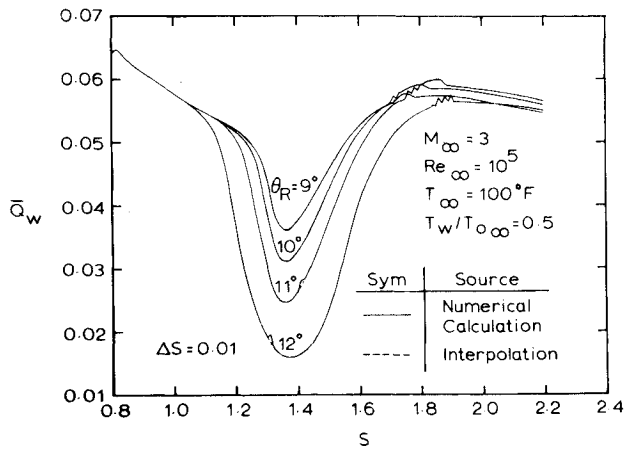

Fig. 5 Interaction heat-transfer distributions for compression ramps.

sometimes could not recover separating solutions if the longitudinal step size was increased. Figure 6 clearly shows that no such behavior is observed using the present approach. However, note should be taken of the large influence of step size on the separated flow case clearly reflecting the first order (Δs) accuracy level of the present algorithm. This truncation error can be traced directly to the region of large surface curvature change at the ramp juncture point ($s = x_o$) and is completely removed when the total displacement body inclination is differenced to obtain edge quantities instead of just the displacement thickness term of Eq. (7a) where $\bar{\theta}_s$ is usually represented analytically.

In the interest of assessing the efficiency of the present algorithm, a study has been conducted of the time step size influence on the convergence rate. Since in its present application, the ADI method is in reality a relaxation scheme, the time step takes on the role of a relaxation parameter. The optimum value of this parameter cannot usually be determined analytically (see Ref. 21 for further discussion of this point) and thus a time step study is in order. The test case chosen was the compression ramp with a $\theta_R = 10°$ which is shown in Fig. 4 to experience a considerable amount of separation. Figure 7 show the results of a time step study for this case in terms of the value of the displacement thickness, δ, at three separate stations along the ramp. It is immediately apparent from all of these figures that the algorithm was reasonably converged for all Δt within 10 iterations. Careful inspection of these figures shows that a time step on the order of $\Delta t = 20$-30 achieves convergence in the 8 to 9 iteration category, this corresponding to approximately 15 min of computer time. For present purposes, the method was usually allowed to proceed to approximately 25 iterations to get a well defined steady state solution throughout the mesh.

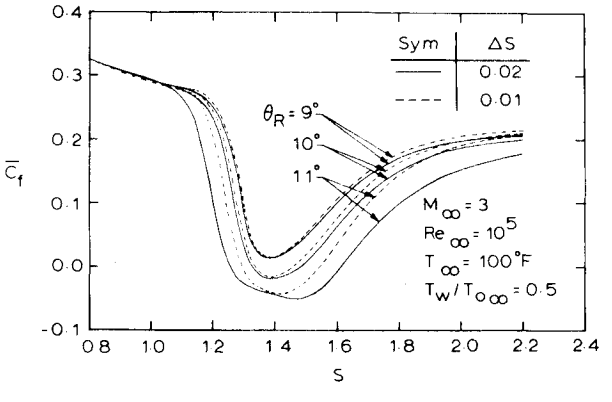

Fig. 6 Mesh size influence on separation solutions.

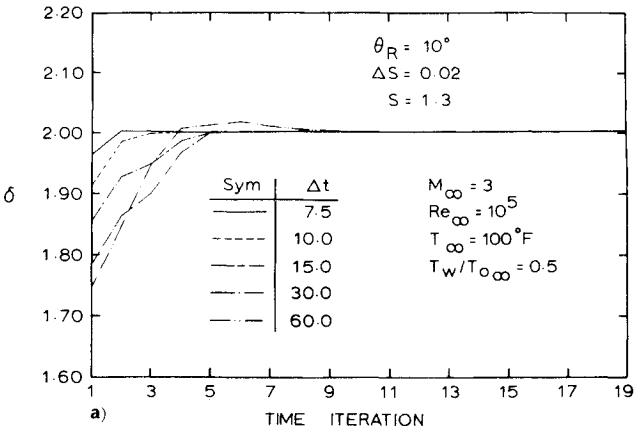

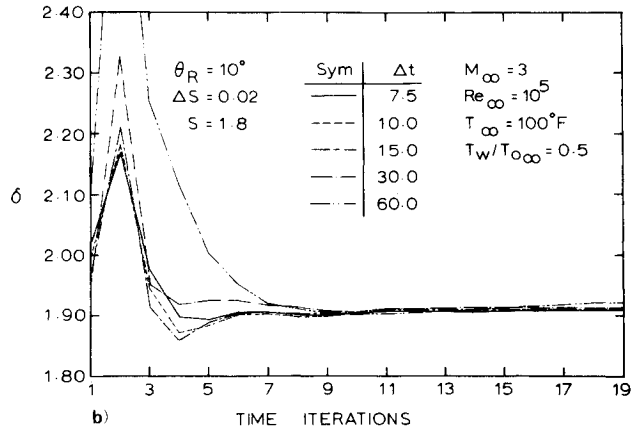

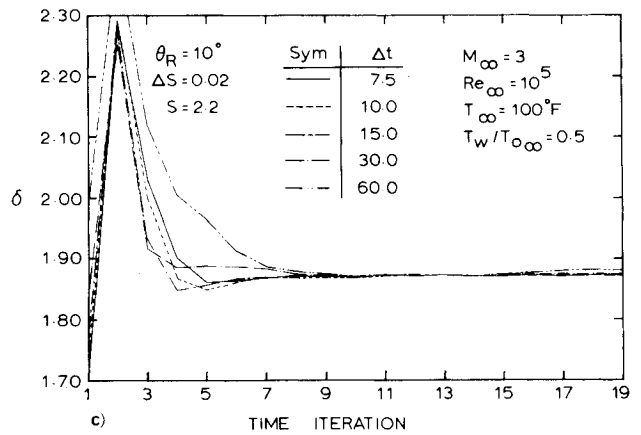

Fig. 7 Time increment influence on ADI convergence rate: a) $S = 1.3$, b) $S = 1.8$, c) $S = 2.2$.

The two test cases chosen for study here are ones for which both Navier-Stokes solutions and experimental data are available for comparison. The test conditions for the first case are: $M_\infty = 4.0$, $Re_\infty = 6.8 \times 10^4$, $T_w = T_{aw}$, and $\theta_R = 10°$. The experimental data is available for these test conditions for a sharp compression corner from Lewis et al.[28] In Ref. 29, Carter presented numerical solutions of the Navier-Stokes equations for the identical flow configuration showing excellent agreement with the data. The smooth compression corner parameters of Fig. 1 were adjusted so that the present geometry reasonably approximated a sharp corner in most of the region except for a small distance near the starting point of the ramp. Figure 8 compares the geometry of the two cases, ($C = 0.14$), as well as the attendant inviscid pressure distributions. For this case, it was found necessary to employ a pressure law more accurate than linear

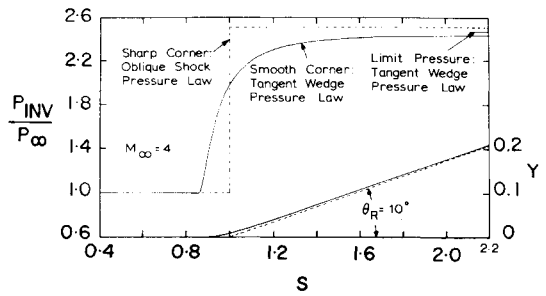

Fig. 8 Ramp geometry and inviscid pressure distribution at $M_\infty = 4$.

theory (note that here $M_\infty = 4$). With simple adjustments, the tangent wedge pressure law was incorporated into the present study producing the inviscid distribution of Fig. 8. Note that the major difference in the two geometries takes place over the region $0.86 \leqq s \leqq 1.2$ and this is reflected in the pressure distributions over the same region.

The calculations were performed from $s = 0.4$ to $s = 2.2$, with $\Delta s = 0.01$ and consumed approximately 30 min of computer time for 25 iterations. At the upstream end, the weak interaction pressure was given as the boundary condition, whereas $\delta'' = 0$ was used at the downstream boundary. The surface pressure obtained from these calculations (for $\Delta s = 0.01$) is presented in Fig. 9, along with the Navier-Stokes solution[29] and the experimental data.[28] Note that the present results compare very favorably ahead of $s = 0.86$, where the weak interaction and free interaction pressure rise takes place. The point of separation predicted by Carter[29] is reproduced in the present study and then some differences are observed over the region $0.86 \leqq s \leqq 1.2$. In light of the differences in the geometry in this region as presented in Fig. 8, this is not considered serious. Aft of $s = 1.2$ the present solution attains a pressure level between that given by the experimental data and the Navier-Stokes solutions. Again, this is not considered serious and the present results are believed below the Navier-Stokes solutions due only to the tangent wedge pressure law and are above the experiments because the latter were performed on an axisymmetric body.

In Fig. 9 a filled circle point is shown at $s = 0.87$ representing the calculated pressure level at the first station on the ramp surface. Note that this pressure level represents a "kink" in the calculated pressure level similar to those observed in Fig. 3. Again this can be traced directly to truncation errors arising from the longitudinal derivative approximations. As shown in Fig. 8, it is in the region of the ramp junction that the inviscid pressure rise experiences a very high longitudinal pressure gradient and this leads to the pressure "kink" observed.

A second test case was studied at $M_\infty = 6$ and comparisons again made with both Lewis' experimental data[28] and Carter's Navier-Stokes solutions.[29] Figure 10 compares the surface geometries (here $C = 0.25$) and surface pressures showing maximum differences again for $0.8 \leqq s \leqq 1.2$. The interacting boundary-layer calculations were performed from $s = 0.3$ to $s = 2.1$ with $\Delta s = 0.01$ and consumed approximately 30 min to perform 25 time iterations. The comparison with experimental

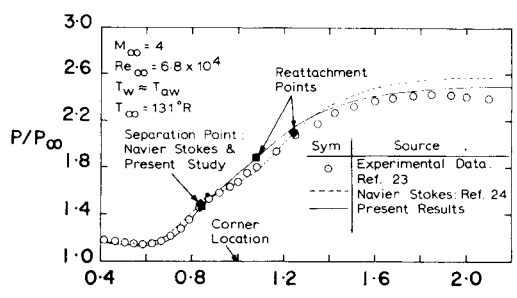

Fig. 9 Comparison of theories and experiments for $M_\infty = 4$.

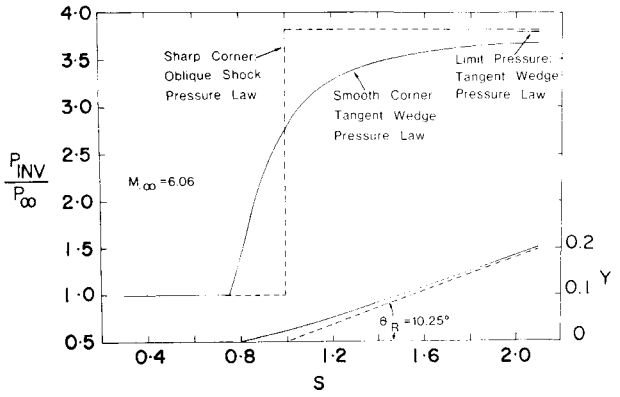

Fig. 10 Ramp geometry and inviscid pressure distribution at $M_\infty = 6$.

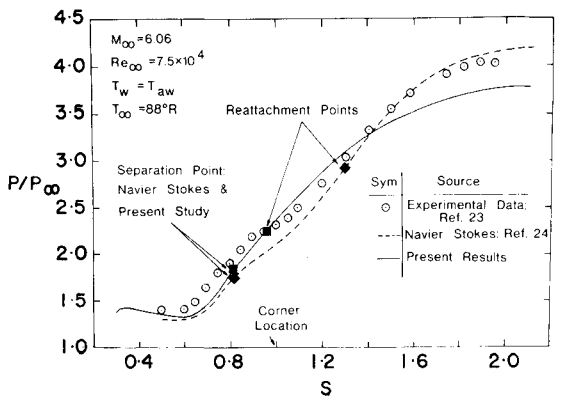

Fig. 11 Comparison of theories and experiments for $M_\infty = 6$.

data is shown in Fig. 11 and is seen to be reasonable considering the differences in geometry noted in Fig. 10. The fact that the present results compare more favorably with the experimental data than Carter's exact solution must be considered fortuitous. The important issue is that the present approach has the capability of directly accounting for the downstream boundary and, in so doing, reasonably well represents the observed flow state.

Conclusions and Recommendations

Based on the comparisons and test cases discussed above, it is concluded that the alternating direction algorithm proposed here provides a reasonably fast means of solving interacting boundary-layer flows with separation. While the computing time required is not considered excessive, it has recently been found that with minor modifications, the computing effort can be reduced to 5–10 min. This was accomplished by moving all the inviscid edge computations into the $n+1$ loop thereby reducing the nonlinearities to be handled during the * loop.

The comparisons shown in Figs. 9 and 11 show that the boundary-layer model, adjusted for interaction effects, produces results competitive with solutions to the full Navier-Stokes. The computational advantage in using the boundary-layer model is quite obvious and is centered in the fact that the inviscid flow, as represented by the edge properties, is directly accounted for in a simple second-order ordinary differential equation. Extension of this concept to subsonic flows introduces a more complicated inviscid pressure law, but nonetheless should be possible via the ADI concept employed here.

References

[1] Lees, L. and Reeves, B. L., "Supersonic Separated and Reattaching Laminar Flows: I General Theory and Application to Adiabatic Boundary-Layer/Shock-Wave Interaction," *AIAA Journal*, Vol. 2, No. 11, Nov. 1964, pp. 1907–1920.

[2] Nielsen, J. N., Lynes, L. L., and Godwin, F. K., "Theory of

Laminar Separated Flows on Flared Surfaces Including Supersonic Flow with Heating and Cooling," *AGARD Conference Proceedings, No. 4*, Separated Flows, 1966.

[3] Holden, M. S., "Theoretical and Experimental Studies of Laminar Flow Separation on Flat Plate-Wedge Compression Surfaces in the Hypersonic Strong Interaction Regime," ARL 67-0112, May 1967, Aerospace Research Labs, Wright-Patterson Air Force Base, Ohio.

[4] Alber, I. E., "Similar Solutions for a Family of Separated Turbulent Boundary Layers," AIAA Paper 71-203, New York, 1971.

[5] Reeves, B. L., "A Two-Layer Model of High Speed Two- and Three-Dimensional Turbulent Boundary Layers with Pressure Gradient and Surface Mass Injection," *AIAA Journal*, Vol. 12, No. 7, July 1974, pp. 932–939.

[6] Reyhner, T. A. and Flügge-Lotz, I., "The Interaction of a Shock Wave with a Laminar Boundary Layer," Rept. 163, Nov. 1966, Div. of Engineering Mechanics, Stanford University, Stanford, Calif.

[7] Werle, M. J., Polak, A., and Bertke, S. D., "Supersonic Boundary-Layer Separation and Reattachment—Finite Difference Solutions," Rept. AFL 72-12-1, Jan. 1973, Dept. of Aerospace Engineering, University of Cincinnati, Cincinnati, Ohio.

[8] Werle, M. J., Vatsa, V. N., and Bertke, S. D., "Sweep Effects on Supersonic Separated Flows," *AIAA Journal*, Vol. 11, No. 12, Dec. 1973, pp. 1763–1765.

[9] Dwoyer, D. L., "Supersonic and Hypersonic Two-Dimensional Laminar Flow Over a Compression Corner," AIAA Computational Fluid Dynamics Conference, Palm Springs, Calif., 1973.

[10] Kuhn, G. D. and Nielsen, J. N., "Prediction of Turbulent Separated Boundary-Layers," AIAA Paper 73-663, Palm Springs, Calif., 1973.

[11] Mikhailov, V. V., Nieland, V. Ya., Sychev, V. V., "The Theory of Viscous Hypersonic Flow," *Annual Review of Fluid Mechanics*, Vol. 3, 1971, pp. 371–396.

[12] Garvine, R. W., "Upstream Influence in Viscous Interacuon Problems," *The Physics of Fluids*, Vol. 11, July 1968, pp. 1413–1423.

[13] Baum, E., "An Interaction Model of a Supersonic Laminar Boundary-Layer on Sharp and Rounded Backward Facing Steps," *AIAA Journal*, Vol. 6, No. 3, March 1968, pp. 440–447.

[14] Werle, M. J., Dwoyer, D. L., and Hankey, W. L., "Initial Conditions for the Hypersonic-Shock/Boundary-Layer Interaction Problem," *AIAA Journal*, Vol. 11, No. 4, April 1973, pp. 525–530.

[15] Stewartson, K. and Williams, P. G., "Self-Induced Separation," *Proceedings of the Royal Society of London*, Ser. A, Vol. 312, Sept. 1969, pp. 181–206.

[16] Messiter, A. F., Feo, A., and Melnik, R. E., "Shock-Wave Strength for Separation of a Laminar Boundary-Layer at Transonic Speeds," *AIAA Journal*, Vol. 9, No. 6, June 1971, pp. 1197–1198.

[17] Brillant, H. M., "Shock-Wave Boundary-Layer Interactions in Laminar Transonic Flow," *AIAA Journal*, Vol. 12, No. 3, March 1974, pp. 323–329.

[18] Van Dyke, M., "Higher Order Boundary Layer Theory," *Annual Review of Fluid Mechanics*, Vol. 1, 1969, pp. 265–292.

[19] Davis, R. T., Werle, M. J., and Wornom, S. F., "A Consistent Formulation of Compressible Boundary-Layer Theory with Second-Order Curvature and Displacement Effects," *AIAA Journal*, Vol. 8, No. 9, Sept. 1970, pp. 1701–1703.

[20] Werle, M. J. and Davis, R. T., "Integral Equations for Incompressible Second-Order Boundary-Layers," *International Journal of Engineering Science*, Vol. 4, No. 4, 1966, pp. 423–431.

[21] Carnahan, B., Luther, H. A., Wilkes, J. A., *Applied Numerical Methods*, Wiley, New York, 1969.

[22] Flügge-Lotz, I. and Blottner, F. G., "Computation of the Compressible Laminar Boundary Layer Flow Including Displacement Thickness Interaction Using Finite Differences Methods," TR 131, 1962, Div. of Engineering Mechanics, Stanford University, Stanford, Calif.

[23] Brown, S. N. and Stewartson, K., "Laminar Separation," *Annual Review of Fluid Mechanics*, Vol. 1, 1969, pp. 45–72.

[24] Werle, M. J. and Senechal, G. D., "A Numerical Study of Separating Supersonic Laminar Boundary Layers," *Journal of Applied Mechanics*, Vol. 4, Series E, No. 3, Sept. 1973, pp. 679–684.

[25] Buckmaster, J., "The Behavior of a Laminar Compressible Boundary Layer on a Cold Wall Near a Point of Zero Skin Friction," *Journal of Fluid Mechanics*, Vol. 44, Pt. 2, 1970, pp. 237–247.

[26] Werle, M. J. and Bertke, S. D., "A Finite-Difference Method for Boundary Layers with Reverse Flows," *AIAA Journal*, Vol. 10, No. 9, Sept. 1972, pp. 1250–1252.

[27] Blottner, F. G., "Finite Difference Methods of Solution of the Boundary-Layer Equations," *AIAA Journal*, Vol. 8, No. 2, Feb. 1970, pp. 193–205.

[28] Lewis, J. E., Kubota, T., and Lees, L., "Experimental Investigation of Supersonic Laminar, Two-Dimensional Boundary-Layer Separation in a Compression Corner with and without Cooling," *AIAA Journal*, Vol. 6, No. 1, Jan. 1968, pp. 7–14.

[29] Carter, J. E., "Numerical Solutions of the Navier-Stokes Equations for the Supersonic Laminar Flow Over a Two-Dimensional Compression Corner," TR R-385, July 1972, NASA.

[30] Werle, M. J. and Vatsa, V. N., "Numerical Solution of Interacting Supersonic Boundary Layer Flows Including Separation Effects," Rept. 73-0162, Dec. 1973, Aerospace Research Laboratories Wright-Patterson Air Force Base, Ohio.